Manuscript version: Author's Accepted Manuscript
The version presented in WRAP is the author's accepted manuscript and may differ from the published version or Version of Record.

Persistent WRAP URL:
http://wrap.warwick.ac.uk/110001

How to cite:
Please refer to published version for the most recent bibliographic citation information.
If a published version is known of, the repository item page linked to above, will contain details on accessing it.

Copyright and reuse:
The Warwick Research Archive Portal (WRAP) makes this work by researchers of the University of Warwick available open access under the following conditions.

Publisher's statement:
Please refer to the repository item page, publisher's statement section, for further information.

For more information, please contact the WRAP Team at: wrap@warwick.ac.uk.

warwick.ac.uk/lib-publications

Experimental investigations on forming limit diagram of ultra thin SS 304 steel: Effect of circular grid size, sheet orientation, punch size and deformation speed

C. Sudarsan[1], K.H. Banker [1], S. Hazra[2], R. Bhagat[2], S.K. Panda[1*]

[1] Department of Mechanical Engineering, Indian Institute of Technology, Kharagpur, West Bengal, India, 721302

[2] Warwick Manufacturing Group, University of Warwick, Coventry, United Kingdom, CV4 7AL

*corresponding author - sushanta.panda@mech.iitkgp.ernet.in

Abstract

In the present work, SS 304 sheet of 200 μm thickness was used to experimentally evaluate the forming limit diagram (FLD). In this context, a sub-size limiting dome height (LDH) test setup was developed to deform rectangular specimens of different widths using a 30 mm hemispherical punch. Further, effect of various parameters such as change in circular grid size, stretching direction with respect to rolling direction of the sheet, punch size and deformation speed on limiting strains was investigated. It was observed that there was marginal change in limiting strains due to the change of punch diameter from 30 mm to 50 mm. The FLD_0 level changed approximately 7.5% and 6.8% with the change in punch diameter and stretching direction respectively. It was also found that the FLD_0 value increased by 15% with change in circular grid diameter from 2.5 mm to 2.0 mm. However, a negligible change in the limiting strains was noted when the grid diameter was further reduced to 1.0 mm. There was negligible change in the FLD_0 level with increase in punch speed from 4 mm/min to 100 mm/min, but approximately 13% decrease was found when the punch speed was further increased to 400 mm/min. Moreover, the LDH, strain distribution and failure strains were also analyzed in context of formability.

Keywords: Ultra thin sheets, SS 304, Forming limit diagram, Limiting dome height, Strain distribution

1. Introduction

Ultra thin sheets have been extensively used in the production of micro features on different devices for the enhancement of heat and mass transfer. Specific examples include the fabrication of bipolar and cooling plates in the fuel cells, micro heat exchangers, micro fluidic devices etc [1,2]. The fabrication of the products from the ultra thin sheet demands better precision and accuracy. The metal forming processes, well known for their high production rate, low energy consumption, maximum material usage, near net shape, consistent product quality and better mechanical properties through work hardening, are claimed to be the most suitable processes to fabricate micro features on the devices [3]. The metal forming process on the macro scale has been well developed, and the forming mechanism has been studied extensively in the recent past. However, the knowledge and the techniques used for the macro forming processes cannot be applied directly to the micro forming process due to significant problems like unknown surface and friction conditions, deformation mechanics, and material behavior due to the so called "size effect" [4,5]. At the micro levels, the material behavior is characterized by presence of fewer grains in the deformed area and hence, the material response depends upon size and orientation of the individual grains [6]. Also, there has been

no standardized practice to characterize the formability of the ultra thin sheets. It is noteworthy that there are very little formability information in terms of forming limit diagrams (FLD), and the forming of the ultra thin sheet metals for the production of micro parts is an important research area [6].

The FLD was first introduced by Keeler and Backofen [7] who developed the right hand side of the FLD and was later extended to the left hand side by Goodwin [8]. The region below the FLD corresponds to the safe strain states and the region above represents failure strain states [8]. The FLD is greatly influenced by different material parameters such as strain hardening coefficient (n-value), strain rate sensitivity index (m-value), anisotropy values (r-values), material thickness etc [9]. Several other process parameters such as the variation in strain rate, temperature, blank holding force, lubrication and stretching orientation of the sheet affected the limiting strains. It had also been found that the FLD was significantly affected by some geometrical parameters like the punch radius, draw bead geometry and grid size [10]. There was no open literature on the comprehensive investigation of these parameters on the limiting strains of the ultra thin sheets. In this regard, a sub-size limiting dome height test setup was designed and developed to evaluate the FLD of SS 304 sheet of 200 μm thickness at room temperature. The effect of change in grid size, orientation of the sheet metal with respect to rolling direction, punch diameter and deformation speed on the limiting strains has been experimentally investigated systematically. Moreover, the strain distribution, limiting dome height, deformation path and failure strains were analyzed to get an insight into the forming behavior.

2. Experimental methodology

In the present work, 200 μm thick stainless steel grade 304 sheets were used. The chemical composition of this material is shown in Table 1. The greater pct. of Cr provides excellent corrosion resistance property and hence this material is very much suitable for the fabrication of bipolar plates in the fuel cells.

Table 1: Chemical composition (% wt.) of SS 304 used in the present work

Material	C	Si	Mn	P	S	Cr	Ni	Mo	N
SS 304	0.06	0.39	1.28	0.037	0.016	18.3	8.6	0.26	0.018

2.1 Tensile test

The formability related mechanical properties of the 200 μm thick SS 304 sheets were evaluated by uniaxial tensile test along the rolling direction (RD), diagonal direction (DD) and transverse direction (TD). The sub-size tensile specimens as shown in Figure 1 were fabricated using wire EDM as per the standards of Defence Metallurgical Research Laboratory, Hyderabad [11, 12]. The tests were carried in all the three directions in a computer controlled 5 kN INSTRON Universal Testing Machine (UTM) at a constant quasi-static deformation speed of 2 mm/min. The load-displacement data obtained were used to plot engineering stress-strain and true stress-strain curves. Different mechanical properties such as the 0.2% yield strength (YS), ultimate tensile strength (UTS), and pct. elongation were evaluated. Also, the Holloman's power law ($\bar{\sigma} = K\bar{\varepsilon}^n$) was used to correlate the true stress-strain curve, and the strain hardening coefficient (n-value) and the strength coefficient (K-value) of the material were evaluated. Anisotropy properties of the material were evaluated in terms of Lankford coefficient (r-value) by deforming the specimen up to a strain value corresponding to 70-80 % of the UTS. The r-value was evaluated along all the three

directions with respect to RD to characterize the r_0, r_{45}, r_{90} values. The strain rate sensitivity index (m–value) was also evaluated from the true stress-strain curve obtained at three different deformation speeds of 4, 100 and 400 mm/min.
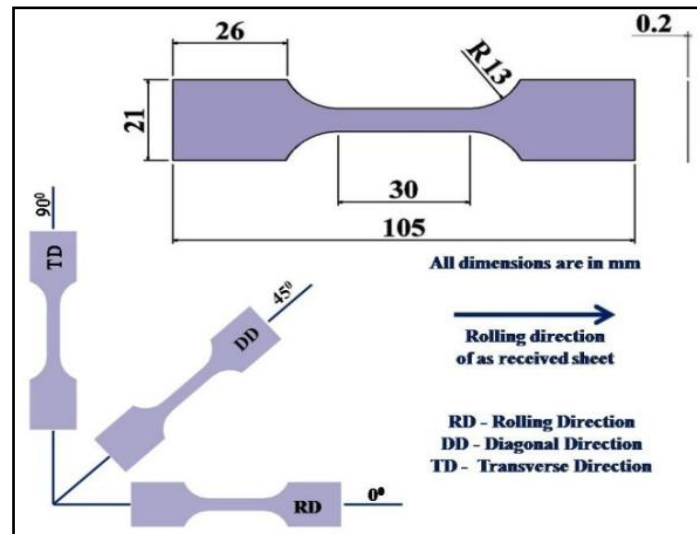

Figure 1. Schematic of the tensile specimen cut with three differently oriented samples (0^0, 45^0, 90^0) with respect to the rolling direction of the sheet

2.2 Limiting dome height test

A sub-size laboratory scale limiting dome height (LDH) test setup was designed and developed consisting of fixture, hemispherical punch of 30 mm diameter, upper and lower dies. The outer diameter of the dies was 150 mm and a circular draw bead was designed in both the dies at 64 mm diameter as depicted in Figure 2 (a). This scaled down LDH test setup was mounted in a UTM of 50 kN capacity. Rectangular specimens were cut from the ultra thin sheet keeping the length of the specimen constant as 80 mm and varying the width in the range from 80 mm – 5 mm in steps of 15 mm. The detailed dimensions of the specimens are shown in Figure 2 (b).
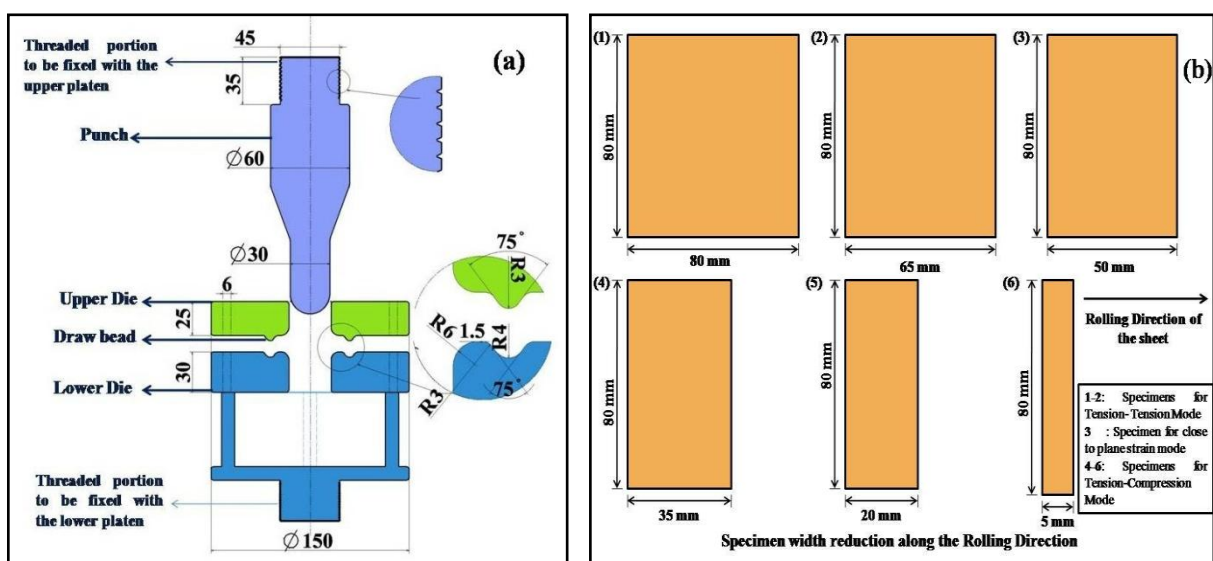

Figure 2. Schematic view of (a) the sub-size LDH test setup and (b) rectangular specimens used for testing

Prior to the LDH test, the specimens were marked with circular grids by the electro chemical etching process. The marked specimens were then clamped tightly between the upper and the lower die with sufficient blank holding force, and the punch was moved down with a constant velocity of 4 mm/min in order to deform the specimens. The test was stopped at the onset of necking/fracture on the deformed cups observed through a mirror placed under the setup. After deformation, the circular grids changed into ellipses. The major and minor diameters of the deformed ellipses were measured using stereo zoom microscope to evaluate both the true major and minor strains. These surface strains were measured in the safe and fracture regions of all the deformed specimens. In this work, circular grid analysis was carried out, and the primary intention was to evaluate the forming limit diagram and the strain distribution profile of the material during the deformation.

All these surface strains were plotted in major and minor strain locus to plot the FLD. The effects of the different parameters such as the circular grid size, orientation of the stretching direction with respect to RD, punch size and deformation speed on the limiting strains of the ultra thin sheets were studied extensively as following.
a) To study the effect of grid size, the specimens were electro chemically etched with circular grid marks of diameter 2.5 mm, 2.0 mm and 1.0 mm.
b) The ultra thin sheets were stretched along the three different orientations such as along 0°, 45°, and 90° with respect to the RD to investigate their effect on the formability.
c) Two different punches of diameter 30 mm and 50 mm were considered to inspect the effect of punch size. It was found that the 50 mm punch LDH test set-up was used previously by Basak and Panda for the formability evaluation of EDD steel sheets [13] and also by Prasad et.al [14] for evaluating the formability of Inconel 718 sheets.
d) The LDH tests were carried out under different punch speeds of 4 mm/min, 100 mm/min, and 400 mm/min respectively to characterize the variation of FLD.
Also, the limiting dome heights, strain distribution profiles, and failure strains were rigorously analyzed.

3. Results and Discussion

3.1 Tensile properties

The true stress-strain responses of the ultra thin sheets of SS 304 tested in all the three directions with respect to the RD are compared in Figure 3 (a). The various tensile properties such as the 0.2% yield strength (YS), ultimate tensile strength (UTS), pct. elongation, strain hardening coefficient (n), strength coefficient (K) were enlisted in Table 2. Further, the plastic anisotropy ratios (r_0, r_{45}, r_{90}) along the three directions, planar anisotropy ($\bar{r} = (r_0 + 2r_{45} + r_{90})/4$), normal anisotropy ($\Delta r = (r_0 - 2r_{45} + r_{90})/2$) were calculated and shown in Table 2.

Table 2: Important mechanical properties obtained from tensile tests in three different orientations of the SS 304 ultra thin sheets

Specimen orientation w.r.t rolling direction	0.2%YS (MPa)	UTS (MPa)	K (MPa)	n	r	$\bar{r}$	Δr	% elongation
0^0	220	705	1480	0.508	0.92			91.3
45^0	215	697	1505	0.516	1.04	0.973	-0.135	98.6
90^0	240	715	1520	0.519	0.89			93.5

There was negligible difference in total elongation along three different orientations (i.e. 0°, 45° and 90°) of the ultra thin SS 304 sheet, and the higher % of elongation was due to the higher *n*-value of this material promoting higher uniform elongation. The $\bar{r}$ value was found to be 0.973 which was very close to isotropy condition. Generally, the increase in *r*-value provides resistance to thinning of material during the deep drawing process. The true stress-strain response of the ultra thin sheets obtained at three different crosshead velocities is shown in the Figure 3 (b). The *m*-value was evaluated at a constant strain of 0.15 using the relation $m = \left[\{\ln(\sigma_2 / \sigma_1)\} / \{\ln(\dot{\varepsilon}_2 / \dot{\varepsilon}_1)\} \right]$, where σ_1 and σ_2 are the flow stresses of the material at corresponding strain rates $\dot{\varepsilon}_1$ and $\dot{\varepsilon}_2$. The strain rate of the material was changed during the jump test by changing the crosshead velocity. It was found that the *m*-value was 0.0008 when the deformation speed was changed from 4 mm/min to 100 mm/min. However, with further increase in the speed to 400 mm/min, the *m*-value was found to increase to 0.046. This result showed that the ultra thin SS 304 sheet was strain rate sensitive at higher crosshead velocities.
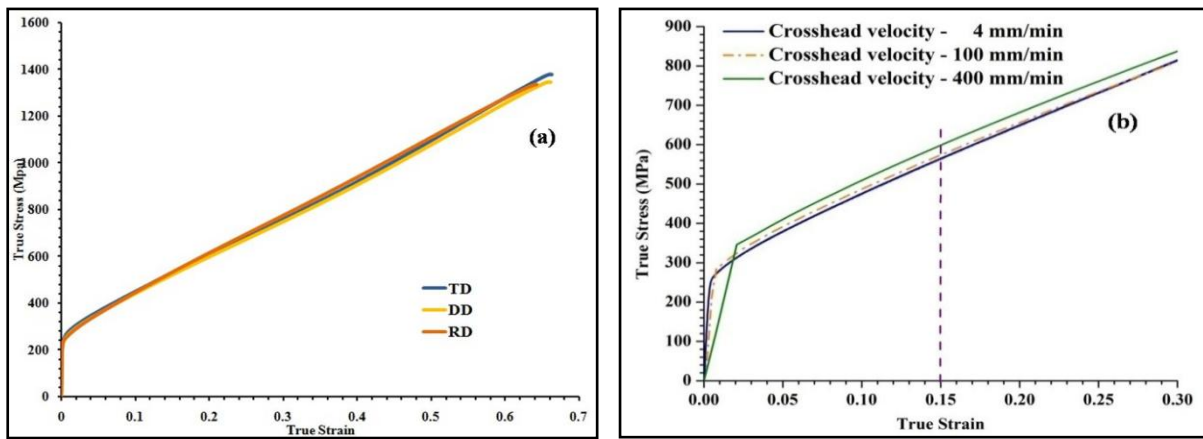

Figure 3. True stress-strain response of SS 304 sheet (a) along the three directions and (b) at different crosshead velocities
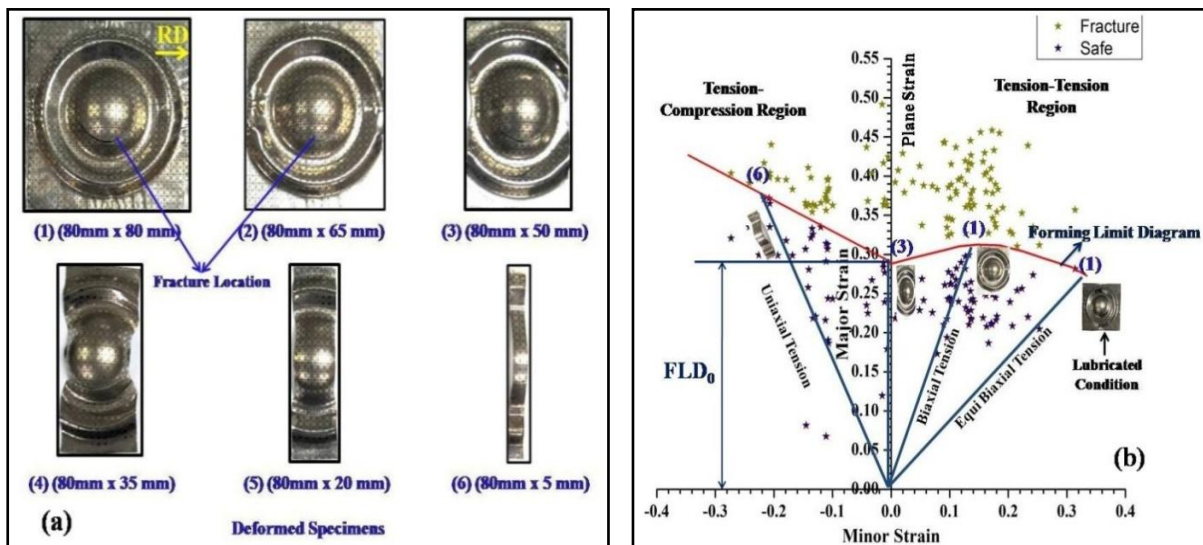

Figure 4. (a) Deformed specimens of different widths and (b) estimated FLD along different strain paths

3.2 Forming limit diagram

The specimens of various widths deformed along the RD using the limiting dome height test have been shown in Figure 4 (a). The true major and minor surface strains corresponding to the different fracture and safe regions of the deformed specimens of the various widths were plotted in the principal strain space with major strain (ε_1) as the ordinate and minor strain (ε_2) as the abscissa. The forming limit diagram (FLD) was constructed separating the fracture regions from the safe region as shown in Figure 4 (b). It can be seen that a series of loading paths ranging from the tension-tension region to the tension-compression region could be achieved using the developed sub-size LDH test setup. Each of these loading paths corresponded to the mode of deformation of a particular width specimen. It can be found that the specimens of widths 80 mm, 50 mm and 5 mm represented the biaxial, close to plane strain and uniaxial deformation paths respectively under dry condition and the 80 mm width specimen represented an equi-biaxial deformation path under lubricated condition. It is noteworthy that the bending strains induced in the specimens have been estimated using Eq. 1. There were previous literatures on the analysis of the bending strains developed due to the use of sub-size punch geometry [14,15]. In the biaxial deformed specimen under lubricated condition, the bending strain was found out to be 0.0045, and this strain was deducted from both the major and minor strains to obtain the corrected limiting strains. Similarly, the limiting strains were corrected for other deformation paths in order to get the corrected FLD. It was found that due to the smaller thickness of the sheet material, the bending strains were very negligible.

$$\varepsilon_{bending} = \ln(1 + \frac{t_f}{2R_n}) \tag{1}$$

Where t_f is the instantaneous thickness at the onset of necking and R_n is the radius of curvature of the middle surface of the sheet. The Y intercept of the FLD with the major strain axis, referred to as FLD_0, as shown in the Figure 4 (b), was also used as the measure of the formability.

3.2.1 Effect of circular grid size

The use of circular grids of diameter of 5.0 mm, 2.5 mm and 3.0 mm for the evaluation of FLD of 1 mm thick sheets had already been reported in the literature previously [16-18]. In the present manuscript, three different circular grids of diameter 2.5 mm, 2.0 mm and 1.0 mm were considered for 200 μm ultra thin SS 304 sheet to conduct the sensitivity analysis of the change in grid dimension on FLD.
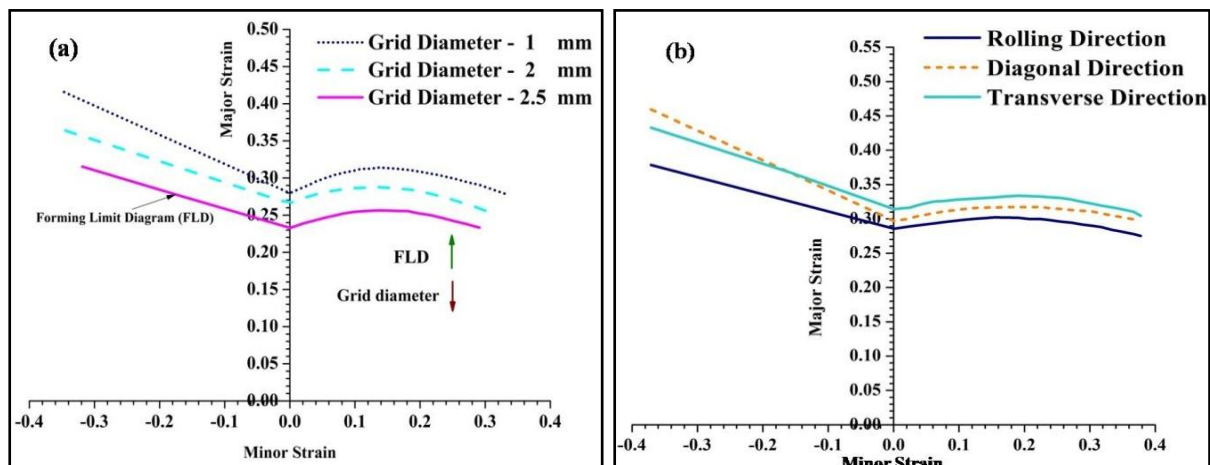

Figure 5. Effect of parameters on the FLD: (a) circular grid size and (b) orientation of stretching direction

The FLDs of SS 304 sheet estimated using three grid diameters of 2.5 mm, 2.0 mm and 1.0 mm are shown in the Figure 5 (a). It can be observed that with decrease in the grid dimension, there was an increase in the FLD_0 level. An increase of approximately 15% in the FLD_0 value was observed when the diameter of the circular grid was changed from 2.5 mm to 2.0 mm. However, a negligible change was found when the grid diameter was changed from 2.0 mm to 1.0 mm. Change in grid dimension greatly affects the limiting strains. It is found that the necking dimension is lower than the grid gauge length and hence, the total true strain is averaged out over the entire deformed ellipse while estimating by the bigger circular diameter. With the decrease in the grid diameter, the total necking/fracture region can be measured more accurately and hence, the limiting strains increased significantly with decrease in grid dimension.

Moreover, with the use of 1.0 mm grid diameter, more number of grids (approximately 30 numbers) were obtained under the deformation region of the punch. Thus, more accurate strain distribution profile was obtained from deformed specimen. With further reduction of the grid diameters, the grid gauge length also decreases due to which inaccuracy in measurement of the limiting strains may be obtained. Therefore, in the present study, 1.0 mm grid size was chosen for further analyses. In future, the digital image correlation (DIC) technique may be used to compare with these experimental data to further enrich the sensitivity analyses.

3.2.2 Effect of orientation of the sheet

The FLDs were evaluated by carrying out the LDH test of specimens cut along RD, DD and TD, and the corresponding limiting strains were compared as shown in Figure 5 (b). A minor change in the limiting strains can be observed over entire strain paths, and the FLD_0 value was found to be maximum for the TD with an increase of approximately 6.78% with respect to that along RD. It can also be seen from the left hand side of the FLD, the limiting strains had a higher value when stretched along DD as compared to the TD and RD. The change in the limiting strains can be attributed to change in the *n*-value and *r*-value of the material in different directions. It was reported in the previous literature [19] that the increase in the *n*-value of the material increases the FLD_0, and the increase in *r*-value changes the slope of the left hand side of the FLD.

3.2.3 Effect of punch size

In order to examine the influence of the punch diameters, two different LDH test setups with punches of diameters 30 mm and 50 mm respectively were used to deform the specimens. In both the setups, the specimens were marked with 1.0 mm circular grids. As the thickness of the sheets being used was in microns, therefore, the bending strains induced were found out to be negligible while deforming by both the punches. The comparison of FLDs estimated using both punches is shown in Figure 6 (a). It could be observed that there was a marginal difference in limiting strains. The LDH test using 50 mm punch was carried out in a 1000 kN hydraulic press using fixture as discussed in previous work [13, 14], and the test using 30 mm punch was carried out in a 50 kN UTM as discussed in Section 2.2. A negligible deviation of FLD_0, of approximately 7.5%, was observed with increase in punch diameter from 30 mm to 50 mm. This marginal variability in FLD was may be due to the selection of different punch diameter and machine during the LDH test. The widths of the specimens were varied from 100 mm to 15 mm in steps of 15 mm keeping the length of 100 mm as constant while deforming by 50 mm punch. The different widths of the specimens induced different strain paths in terms of ratio of minor strain (ε_2) to that of major strain (ε_1) during deformation.

This was achieved due to different quantity of lateral drawing of the material into die cavity. The strain ratio during deformation is defined as $\alpha = \varepsilon_2 / \varepsilon_1$. It was found that the strain path changed from $\alpha = 0.45$ to $\alpha = -0.35$ by changing the width of the specimens from 100 mm to 15 mm. In the present work, the different strain paths were also generated using the 30 mm sub-size LDH test setup while deforming various sample widths as shown in Figure 6 (b).
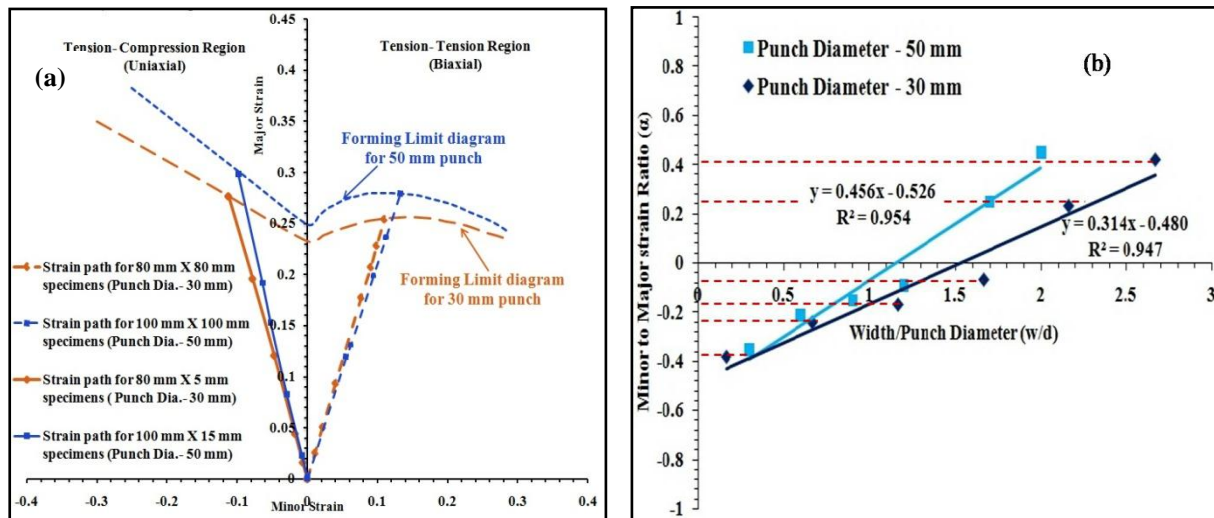

Figure 6. (a) Comparison of FLD evaluated using different punch size and (b) variation of the strain ratio for different width to punch diameter ratio

The nature of the loading path while deforming the specimens using the different punch diameters was also investigated. Two different width specimens representing the biaxial and uniaxial deformation modes were considered for the two punches of diameters 30 mm and 50 mm. The strain path evolved during the deformation of the considered specimens for the two punches has been shown in the Figure 6 (a). The strain path was evaluated using the following steps (i) the failure region was identified and the load displacement data of the deformed cup were obtained after the LDH test, (ii) the maximum load attained prior to fracture was noted, and the dome test was planned to be stopped intermittently at five stages, (iii) at each stage, the specimen was removed from the LDH test set up, and both the major and minor strains at the identified region (failed region) were measured by circular grid analysis, and (iv) the evaluated major and minor strain data of identified region at all five stages were interposed inside the FLDs. These data points were further connected to each other to generate the strain path. It can be observed that linear strain paths could be achieved in all the cases. The strain ratios corresponding to these strain paths were almost similar and very marginal deviation could be observed. There was a marginal change in the FLD_0 with the variation of the punch diameter. Also, the strain paths obtained while deforming specimens of different widths by 30 mm punch were in close agreement with those of the 50 mm punch. Therefore, 30 mm punch diameter was constantly used for other stretch forming experiments.

3.2.4 Effect of deformation speed

To study the effect of deformation speed on the limiting strains, the ultra thin sheets were deformed with three different crosshead velocities of 4 mm/min, 100 mm/min and 400 mm/min respectively. The FLDs of the corresponding punch velocities are shown in Figure 7 (a). The formability of the ultra thin sheets can be found to be greatly affected by the deformation speed. The FLD_0 level reduced with increase in deformation speed and

approximately 16% reduction was observed when punch speed was changed from 4 mm/min to 400 mm/min.
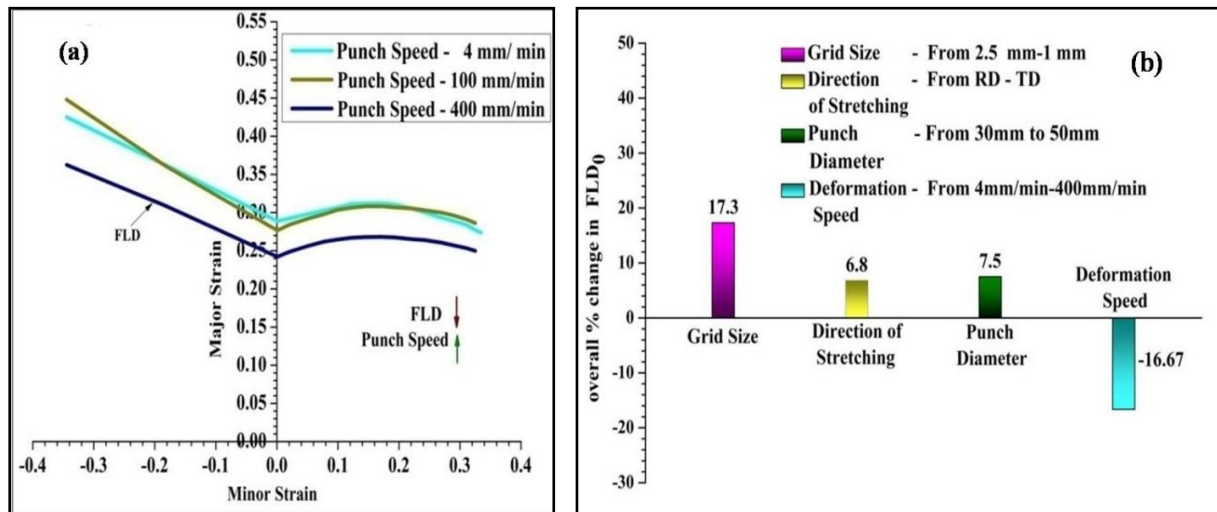

Figure 7.(a) Effect of deformation speed on the FLD and (b) effect of different parameters on the overall % change in FLD_0

All the FLDs considering different parameters were plotted, and the comparative effect of the parameters on the overall pct. change in the FLD_0 has been presented in the Figure 7 (b). It could be inferred that the limiting strains were very much sensitive to the change in grid size and the deformation speed. A negligible effect of both stretching direction and punch diameter on the limiting strains was observed.

3.3 Limiting dome height

The dome heights of the deformed specimens obtained at the onset of necking and fracture were measured. Table 3 summarizes the comparison of the experimental LDH for two different punch diameters and three different deformation speeds.

Table 3: Limiting dome height comparison using different punch diameters and deformation speeds

Specimen geometryused for different punch (in mm×mm)		Strain Ratio (α)	LDH obtained from different punch size (in mm)		LDH obtained from different deformation speeds tested using 30 mm punch (in mm)		
30 mm punch	**50 mm punch**		**30 mm punch**	**50mm punch**	**4mm/min**	**100mm/min**	**400mm/min**
80×80	100×100	0.45	14.75±0.07	21.98±0.08	14.75±0.07	13.95±0.08	12.75±0.07
80×65	100×85	0.25	13.75±0.08	21.18±0.09	13.75±0.08	12.75±0.07	11.75±0.03
80×50	100×60	-0.07	13.25±0.08	20.98±0.07	13.25±0.08	12.15±0.05	11.15±0.07
80×35	100×45	-0.15	13.65±0.07	20.77±0.08	13.75±0.07	12.05±0.06	11.05±0.06
80×20	100×30	-0.21	13.95±0.09	20.95±0.09	13.95±0.09	12.25±0.07	11.75±0.09
80×5	100×15	-0.35	14.05±0.09	21.75±0.07	14.05±0.09	12.75±0.09	12.08±0.07
80×80 (Lub)	100×100 (Lub)	0.85	15.75±0.07	23.75±0.07	15.75±0.07	14.75±0.07	13.75±0.07

The stretching orientation of the sheet did not have much effect on the dome heights and it was averaged out. It could be found from the table that dome height increased with the

increase in the punch diameter. However, the overall ratio of the dome height to the punch diameter was found to remain almost similar in both the cases. The dome heights were also evaluated at three different crosshead velocities. A decreasing trend was observed with increase in the deformation speed and it was due to the decrease in the limiting strains.

3.4 Fracture strain and strain distribution profile

The failure locations of the specimens were identified and Hill's 48 anisotropy yield theory was used to find out the effective plastic failure strain (EPFS) using Eq.2. The effective failure strain was estimated from the measured true major (ε_1), and minor strain (ε_2) of the failure location and the corresponding thickness strain (ε_3) was evaluated using the concept of volume constancy ($\varepsilon_1 + \varepsilon_2 + \varepsilon_3 = 0$).

$$\bar{\varepsilon} = \left[\left\{ \frac{r_{90}(1 + r_0)}{(r_{90}.r + r_{90}.r_0^2 + r_{90}^2.r_0)^2} \right\} \left\{ r_0(r_{90}.\varepsilon_2 - r_0.r_{90}.\varepsilon_3)^2 + r_{90}(r_{90}.r_0.\varepsilon_2 - r_{90}.\varepsilon_3)^2 + r_0.r_{90}(r_0.\varepsilon_1 - r_{90}.\varepsilon_2)^2 \right\} \right]^{1/2} \quad (2)$$
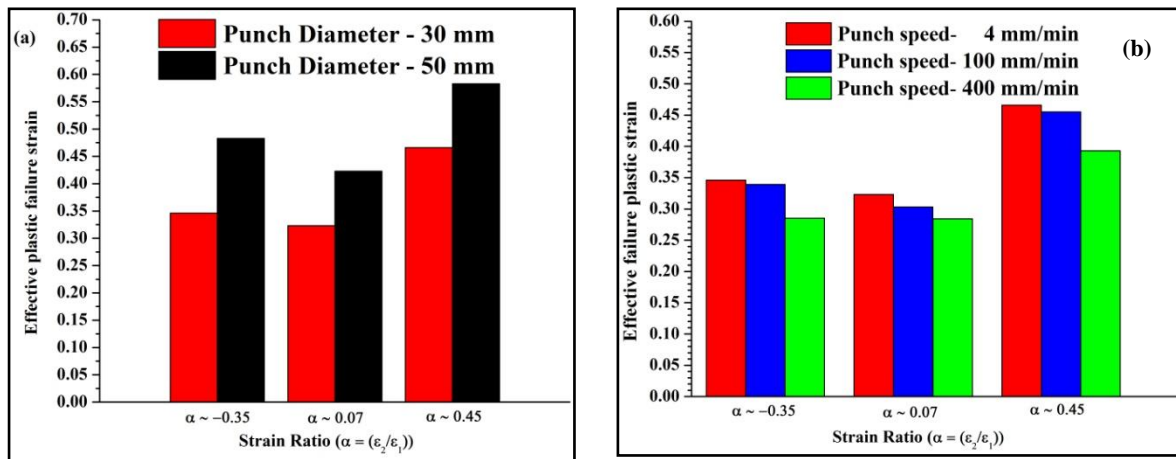

Figure 8. The equivalent plastic failure strain evaluated for (a) different punch size and (b) different deformation speeds

The change in the grid dimension and stretching orientation did not mark any specific difference in the failure strain. However, there was again a significant effect of the change in punch diameter and deformation speed on the effective failure plastic strain. Figure 8 (a) and (b) depict the effective plastic failure strain (EPFS) evaluated from the LDH test using punches of diameter 30 mm and 50 mm and deformation speeds of 4 mm/min, 100 mm/min, and 400 mm/min. The EPFS for the two different punch diameters was calculated considering the bending strain induced during deformation. It was found that the failure plastic strain increased with the increase in the punch diameter and decreased with increase in the deformation speed under all three deformation paths.

The true major and minor strains were measured on surface of the specimens of different dimensions such as 80 mm×80 mm, 80 mm×50 mm and 80 mm×5 mm corresponding to the biaxial, close to plane strain and uniaxial conditions respectively. These data points were plotted with respect to the distance from the pole to represent the strain distribution profile. Figure 9 represents the specimen deformed along biaxial tension deformation path. The highest point on the dome of the specimen is often referred as pole. The surface major and minor strains along the pole are evaluated using the circular grid analysis method, and are then plotted with respect to the distance from the pole to represent strain distribution profile.
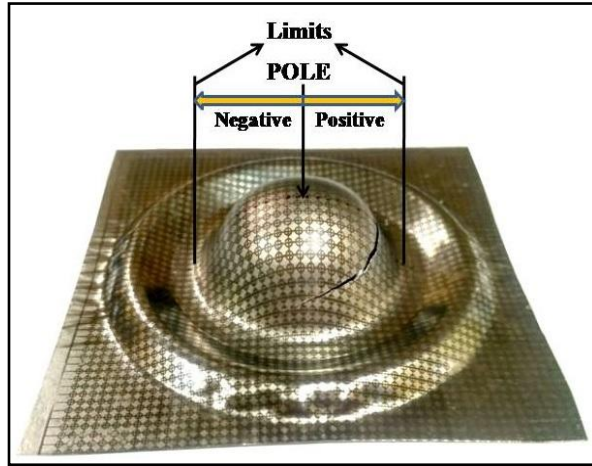
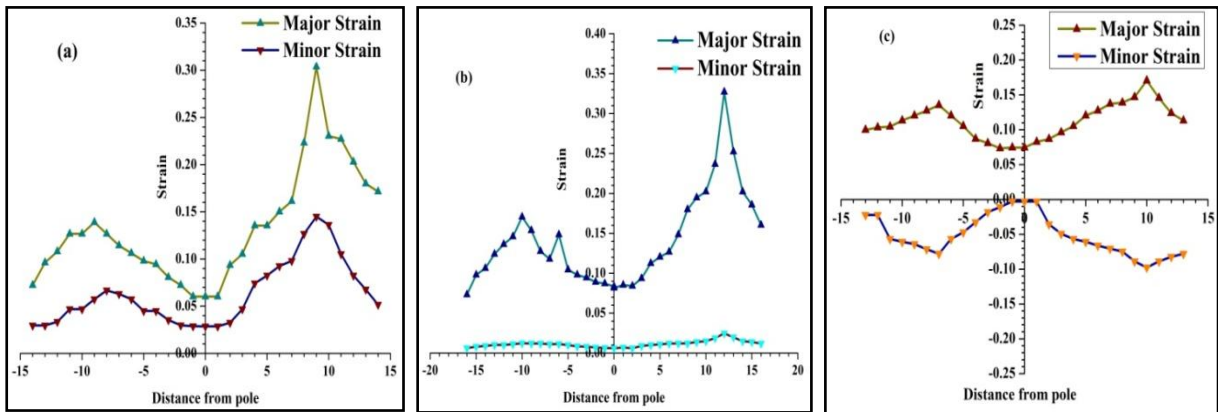**Figure 9.** Specimen deformed along biaxial tension deformation path during the LDH test depicting the pole

Figure 10. Strain distribution profiles obtained for specimen: (a) 80mm×80mm (b) 80mm×50mm and (c) 80mm×5mm

Figure 10 shows the strain distribution profile for the deformed specimens using the punch of diameter 30 mm. From the figure, two peaks can be observed on both sides of the pole in both the major and minor strain distribution profile. The large peak corresponds to the point where fracture had taken place due to strain localization.

It can be found from Figure10 (a) that both major and minor strains were positive indicating biaxial / tension-tension deformation mode for 80 mm ×80 mm specimen. The minor strain can be seen to be very negligible confirming the close to plane strain condition in Figure 10 (b) for 50 mm width specimen. Figure 10 (c) depicts the strain distribution profile of the 5 mm width specimen corresponding to the tension-compression deformation mode. The negative minor strain was due to the excessive lateral drawing of the material during LDH test. It can be found that the major and minor strain distribution depends on the selection of the width of the specimen due to induction of different deformation paths.

4 Conclusions

Based on the results and discussions, the following conclusions were made:

1. The limiting strains were sensitive to the change in the circular grid diameter. The FLD_0 increased by approximately 15% and 17.3% with change in grid diameter from 2.5 mm to 2.0 mm and 2.5 mm to 1.0 mm respectively.
2. As $\bar{r}$ value of the material was found to be close to isotropic condition, the stretching of sheet in different orientations with respect to rolling direction had no significant effect on the forming limits.
3. The limiting strains were found to change with the punch diameter. The maximum difference of approximately 7.5% was observed near to plane strain region (FLD_0) when the punch diameter was changed from 30 mm to 50 mm.
4. With increase in deformation speeds from 4 to 400 mm/min, the limiting strains were found to decrease by 16.67%. This decrease in FLD limit might have occurred due to higher strain rate sensitivity of the ultra-thin SS 304 sheets.

References

[1]   Y. Qin, Micro-forming and miniature manufacturing systems - development needs and perspectives, J. Mater. Process. Technol. 177 (2006) 8–18.
[2]   Y. Liu, L. Hua, Fabrication of metallic bipolar plate for proton exchange membrane fuel cells by rubber pad forming, J. Power Sources. 195 (2010) 3529–3535.
[3]   U. Engel, R. Eckstein, Microforming—from basic research to its realization, J. Mater. Process. Technol. 125–126 (2002) 35–44.
[4]   J. T. Gau, P. H. Chen, H. Gu, R. S. Lee, The coupling influence of size effects and strain rates on the formability of austenitic stainless steel 304 foil, J. Mater. Process. Technol. 213 (2013) 376–382.
[5]   S. Mahabunphachai, M. Koç, Investigation of size effects on material behavior of thin sheet metals using hydraulic bulge testing at micro/meso-scales, Int. J. Mach. Tools Manuf. 48 (2008) 1014–1029.
[6]   H.J. Bong, F. Barlat, M. G. Lee, D. C. Ahn, The forming limit diagram of ferritic stainless steel sheets: Experiments and modeling, Int. J. Mech. Sci. 64 (2012) 1–10.
[7]   S.P. Keeler, W.A. Backofen, Plastic instability and fracture in sheets stretched over rigid punches, Asm Trans Q. 56 (1963) 25–48.
[8]   G.M. Goodwin, Application of strain analysis to sheet metal forming problems in the press shop, SAE Tech. Pap. 60 (1968) 764–774.
[9]   D. Banabic, Sheet Metal Forming Processes, 2010.
[10] F. Casari, M. Tassan, A. Messina, A. Molinari, Effect of punch diameter, grid dimension, and lubrication on forming limit diagram, J. Test. Eval. 34 (2005) 24–30.
[11] A. K. Gupta, V. K. Anirudh, S. K. Singh, Constitutive models to predict flow stress in Austenitic Stainless Steel 316 at elevated temperatures, Mater. Des. 43 (2013) 410-418.
[12] K. S. Prasad, A. K. Gupta, A constitutive description to predict high-temperature flow stress in austenitic stainless steel 316. Procedia materials science, 6 (2014) 347-353.
[13] S. Basak, S. K. Panda, Implementation of Yld96 anisotropy plasticity theory for estimation of polar effective plastic strain based failure limit of pre-strained thin steels, Thin-Walled Struct. (2016) 1–12.
[14] K. S. Prasad, S. K. Panda, S. K. Kar, M. Sen, S. N. Murty, S. C. Sharma, Microstructures, Forming Limit and Failure Analyses of Inconel 718 Sheets for

Fabrication of Aerospace Components, J. Mater. Eng. Perform. 26 (2017) 1513–1530.

[15] S. S. Panicker, H. G. Singh, S. K. Panda, R. Dashwood, Characterization of Tensile Properties, Limiting Strains, and Deep Drawing Behavior of AA5754-H22 Sheet at Elevated Temperature, J. Mater. Eng. Perform. 24 (2015) 4267–4282.

[16] Y. Lou, H. Huh, S. Lim, K. Pack, New ductile fracture criterion for prediction of fracture forming limit diagrams of sheet metals, Int. J. of Solids Struct. 49 (2012), 3605-3615.

[17] J. Min, L. G. Hector, J. Lin, J. T. Carter, Analytical method for forming limit diagram prediction with application to a magnesium ZEK100-O alloy. J. Mater.Eng. Perform. 22 (2013) 3324-3336.

[18] M. Janbakhsh, F. Djavanroodi, M. Riahi, A comparative study on determination of forming limit diagrams for industrial aluminium sheet alloys considering combined effect of strain path, anisotropy and yield locus, J. Strain Anal Engg. Des. 47 (2012) 350-361.

[19] W. M. Sing, K. P. Rao, Role of strain-hardening laws in the prediction of forming limit curves, J. Mater. Process. Technol. 63 (1997) 105–110.